ADVANCED FUNCTIONAL MATERIALS
www.afm-journal.de

Sub-5 nm Dendrimer Directed Self-Assembly with Large-Area Uniform Alignment by Graphoepitaxy

*Kangho Park, Woo-Bin Jung, Kiok Kwon, Oleg D. Lavrentovich, and Hee-Tae Jung**

Directed self-assembly (DSA) using soft materials is an important method for producing periodic nanostructures because it is a simple, cost-effective process for fabricating high-resolution patterns. Most of the previously reported DSA methods exploit the self-assembly of block copolymers, which generates a wide range of nanostructures. In this study, cylinders obtained from supramolecular dendrimer films with a high resolution (<5 nm) exhibit planar ordering over a macroscopic area via guiding topographical templates with a high aspect ratio (>10) and high spatial resolution (≈20 nm) of guiding line patterns. Theoretical and experimental studies reveal that this property is related to geometrical anchoring on the meniscus region and physical surface anchoring on the sidewall. Furthermore, this DSA of dendrimer cylinders is demonstrated by the non-regular geometry of the patterned template. The macroscopic planar alignment of the dendrimer nanostructure reveals an extremely small feature size (≈4.7 nm) on the wafer scale (>16 cm^2). This study is expected to open avenues for the production of a large family of supramolecular dendrimers with different phases and feature dimensions oriented by the DSA approach.

1. Introduction

The directed self-assembly (DSA) of soft materials such as block copolymers (BCPs),[1] colloids,[2] liquid crystals,[3] and supramolecules[4] has received substantial attention for the generation of highly ordered and densely packed nanostructures. DSA techniques have previously been used to fabricate high resolution BCP nanopatterns, which can overcome resolution limitations present in top-down lithographic approaches. The DSA of BCPs provides periodic nanostructures with features 3–50 nm in size according to the microphase-segregation of incompatible polymeric blocks.[5,6] The organized alignment of BCPs can be induced by the use of different DSA techniques involving chemical patterns,[7] neutral surfaces,[8] top-coats,[9] topographical patterns,[10] nano-confinement,[11] mechanical shearing forces,[12] electric fields,[13] and magnetic fields.[14] These DSA processes of BCPs generate highly periodic nanostructures with a low defect level,[15] and result in dense areal packing of nanopatterns with a feature size of sub-10 nm.[16]

Among the various soft building blocks, supramolecular dendrimers are remarkably attractive due to their advantageous properties such as small feature sizes (ranging from approximately 1 nm to around 10 nm), diversity in chemical functionality, and fast ordering times (in the order of min) to self-assembly.[17] The challenges for supramolecular structures that can be used as the template for nanolithography are orientation control, thin film formation, and pattern transfer. In the beginning, the orientation of the dendrimer materials has to be controlled in a monolayer over a large area. In the next step, lithographic methodologies for selective etching, such as selective metal fixation[18] and selective polymerization,[19] have to be followed. After enhancing the etching contrast of monolayer dendrimer films, the pattern transfer should be carried out for the creation of metal nanopatterns and inorganic arrays. For achieving precise pattern transfer to a substrate, highly oriented supramolecular structures over large areas are required. It has been shown that the orientation of the supramolecular structures can be controlled using surface anchoring,[20] geometrical confinement,[21,22] and external fields.[23] These techniques have generated the planar or homeotropic orientation of self-assembled small molecules.[4] There have been studies that examine the planar ordering of liquid crystalline structures with sub-5 nm periodicities.[24] Supramolecular structures with a sub-5 nm feature size can be oriented, but the development of large-area alignment control is essential in order to apply these self-assembling nanostructures to the future high-resolution bottom-up lithography.

In this study, we reported a planar ordering of cylindrical structures (diameter ≈4.75 nm) based on dendrimers over a

K. Park, Dr. W.-B. Jung, Dr. K. Kwon, Prof. H.-T. Jung
Department of Chemical and Biomolecular Engineering
Korea Advanced Institute of Science and Technology (KAIST)
Daejeon 34141, Republic of Korea
E-mail: heetae@kaist.ac.kr
K. Park, Dr. W.-B. Jung, Dr. K. Kwon, Prof. H.-T. Jung
KAIST Institute for NanoCentury
Korea Advanced Institute of Science and Technology (KAIST)
Daejeon 34141, Republic of Korea
Dr. K. Kwon
Green Chemistry and Materials Group
Research Institute of Sustainable Manufacturing System
Korea Institute of Industrial Technology
Cheonan 31056, Republic of Korea
Prof. O. D. Lavrentovich
Liquid Crystal Institute
Kent State University
Kent, OH 44240, USA
The ORCID identification number(s) for the author(s) of this article can be found under https://doi.org/10.1002/adfm.201901876.

DOI: 10.1002/adfm.201901876

macroscopic area (4 cm x 4 cm) in thin films by topographical templates with high-aspect-ratio (>10) and high-resolution (≈20 nm) line patterns. We further controlled the ratio of dendrimer film thickness to guiding pattern height, then confirmed different orientations of dendrimer cylinders. There were two competing mechanisms, geometrical anchoring and physical surface anchoring, which determined the alignment direction of dendrimer cylinders. Furthermore, we examined DSA of cylindrical structures by using curved line patterns.

2. Results and Discussion

2.1. Alignment of Dendrimer Cylinders with High Aspect Ratio Line Patterns

Figure 1 shows the procedure for preparing well-aligned cylinders from supramolecular dendrimer films with a long-range lateral order by graphoepitaxy. In this study, a taper-shaped dendrimer material (Figure 1a) comprising a long aliphatic tail group was examined, which has been reported to form a stable cylindrical structure.[22] Notably, previous experiments have verified that this technique is not limited to a specific supramolecular material, and a large family of dendrimers with different chemistries and feature dimensions can be used. The dendrimer material used herein can be spin-coated in various solvents, which is advantageous for the fabrication of a large-area uniform film on a substrate and for the simple control of film thickness. High-resolution (width (w) ≈20 nm) Au line patterns with different spacings (spacing between lines (s) ≈500 nm–10 μm) and different heights ((h) ≈130–250 nm) were used as guiding templates, which were prepared by secondary sputtering lithography (SSL) (Figure S3, Supporting Information).[25] These high-resolution line templates provided minimal dead spaces (≈1%), which are considerably less than those of conventional microchannels (≈50%). In addition, the high aspect ratio of the line patterns is advantageous for controlling the anchoring energy.[26] Different metals or semiconductors aside from gold can be used as guiding templates provided that different metals or semiconductors can be deposited onto a substrate. A ≈120-nm-thick supramolecular dendrimer film was obtained by spin-casting a 1 wt% dendrimer solution in chloroform onto the line patterns without additional surface treatment. By cooling the dendrimer film from its isotropic melt (87 °C) to room temperature at a rate of ≈1 °C min^{-1}, cylinders with a parallel alignment were obtained (Figure 1b).

Atomic force microscopy (AFM) images revealed the long-range planar alignment of highly ordered dendrimer cylinders in the presence of a high-resolution Au line template (width (w) ≈20 nm, space (s) ≈2 μm, and height (h) ≈250 nm) (Figure 1c). The cylinders were coherently aligned, and the cylinder axes were parallel to the patterned line axis over the entire substrate surface. Even at the interfaces between the dendrimer cylinders and line templates, the alignment direction of the cylindrical structures was parallel to the direction of the line pattern (Figure S4, Supporting Information). Variations in surface profile observed in the height-mode AFM, were on the scale of a few nanometers and were driven by the variation in thickness of the dendrimer film during heating and cooling. The corresponding fast Fourier transform (FFT) pattern clearly revealed two spots, and the line connecting the two spots was perpendicular to the patterned line direction, indicative of the parallel alignment of the cylinders with respect to the guiding line template axis. A high-magnification AFM image confirmed that the cylinders with a d ≈4.75 nm were highly elongated along the line template axis (inset of Figure 1c).

Notably, highly ordered cylinders, which were parallel to the patterned line axis, were consistently produced over the entire guiding template area (4 cm × 4 cm). **Figure 2** shows the long-range ordering of the cylinders, which were oriented parallel to the line pattern, over a centimeter-scale wafer. High-aspect-ratio line templates (w ≈20 nm, s ≈2 μm, and h ≈250 nm) were fabricated (Figure 2a), then a ≈120-nm-thick dendrimer film was casted onto the line patterns (4 cm × 4 cm) and annealed after cooling the film from its isotropic melt state to room temperature at a rate of ≈1 °C min^{-1}. To investigate the order and orientation of the supramolecular dendrimer cylinders, which were created on the patterned area, polarized optical microscopy (POM) images were recorded (Figure 2b). A uniform color under the crossed polarizer was observed within the patterned area, indicative of the uniform alignment of the cylinders, whereas a fan-shaped texture, which was characteristic of a cylindrical liquid crystalline phase, was observed in the non-pattered region, indicative of non-uniform alignment. The orientation of the cylinders on the patterned area was further examined by POM images in the presence of a 530 nm 1λ wave plate at rotations of −45° and +45° to the polarizer. By the rotation of the line pattern filled with dendrimer cylinders at −45° to the polarizer, a blue color was observed, whereas at a rotation of the line direction +45° to the polarizer in the presence of the 1λ wave plate, a red color was observed. This result indicates that the dendrimer cylinders are parallel to the patterned line axis.[27]

Grazing-incidence small-angle X-ray scattering (GISAXS) analysis (Figure 2c) was carried out to obtain precise evidence regarding the uniform planar alignment of the dendrimer cylinders within the line pattern with long-range ordering. With the penetration of the incidence X-ray beam into the patterned line axis (left of Figure 2c), a clear three-point diffraction pattern (i.e., Miller indices [100], [110], and [0–10] of a 2D hexagonal cylinder) was observed at q ≈1.311 nm−1 (period ≈4.79 nm). Only a [100] (q ≈1.303 nm−1, period ≈4.82 nm) stacking peak was observed when the incident X-ray beam penetrated perpendicular to the patterned line axis (right of Figure 2c). A diffraction pattern around the beam stopper corresponded to the scattering of an incident X-ray beam on the wall of the guiding patterns. GISAXS results confirmed that the dendrimer cylinders are coherently aligned parallel to the line pattern over large areas.

Planar-aligned dendrimer cylinders were directly observed by AFM analysis within the guiding template area (Figure 2d). Bright and relatively dark regions in the AFM image revealed the patterned Au lines and dendrimer film, respectively. To investigate the alignment direction of the dendrimer cylinders along the patterned line axis, FFT patterns of the AFM image were recorded at five positions (red spots) along a straight line. As shown in each FFT pattern, the dendrimer cylinders exhibited the same orientation along the patterned line axis. In addition,

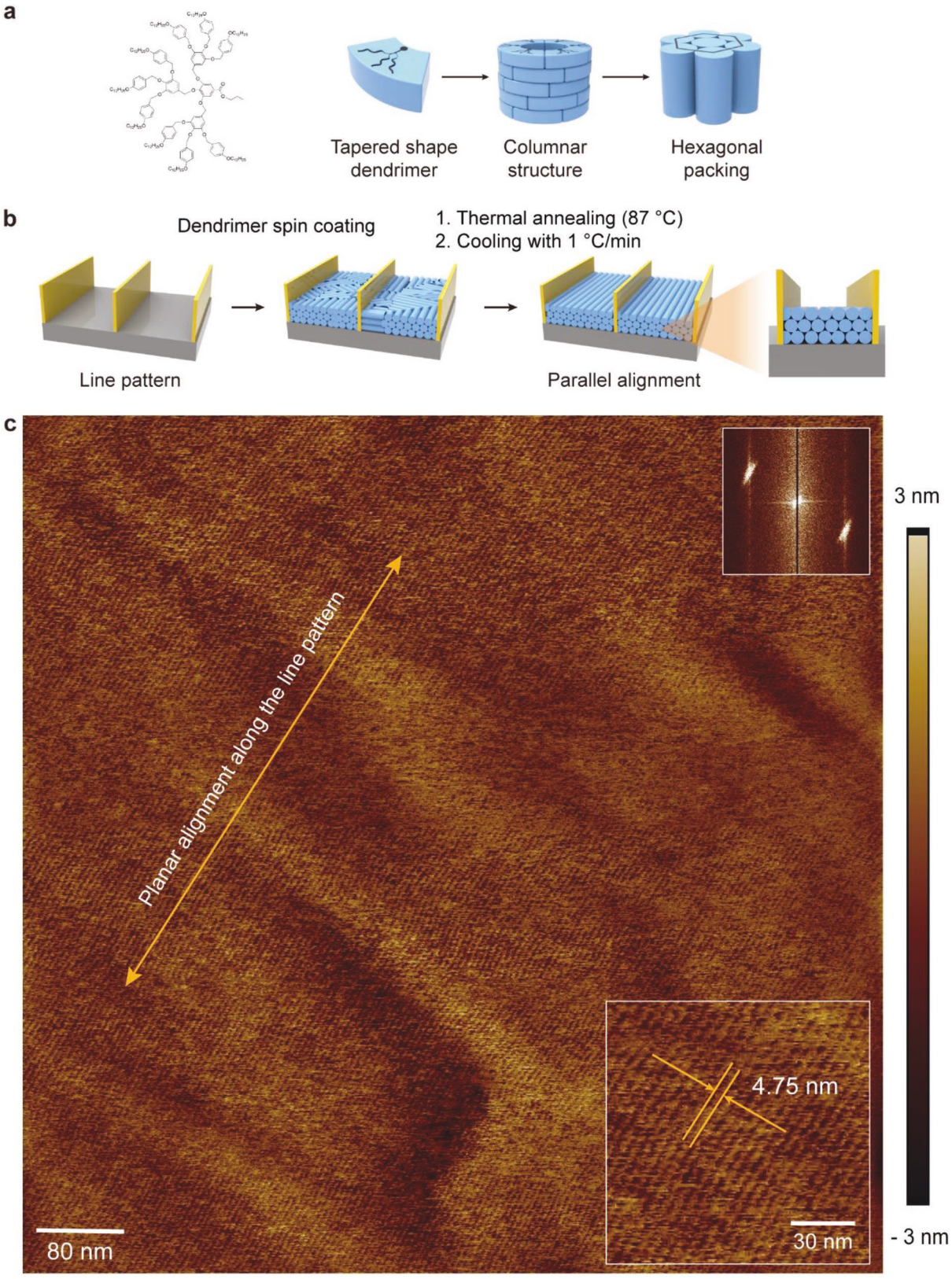

Figure 1. Self-assembly and alignment control of dendrimer cylinders, and characterization. a) Molecular structure and self-assembly of the dendrimer material used. b) Schematic of the aligning dendrimer cylinders confined on the patterned area (width of 20 nm, space of 2 µm, and height of 250 nm). c) AFM image of the dendrimer cylinders along line patterns. Insets show the corresponding FFT and magnified images.

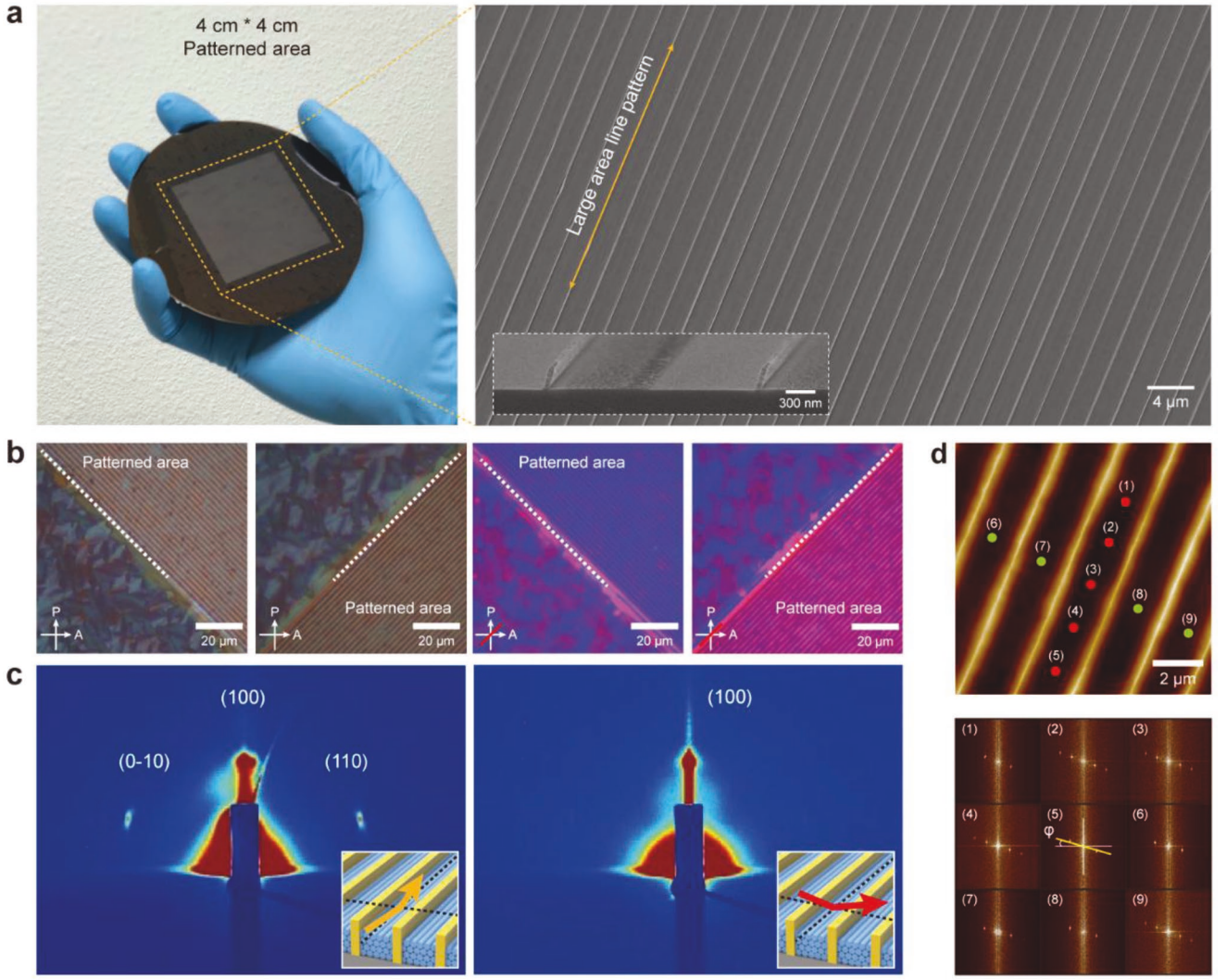

Figure 2. Large-area alignment of dendrimer cylinders with planar ordering. a) Photograph of a dendrimer film on 4 cm × 4 cm patterned area and the SEM image of the high-aspect-ratio line patterns (width of 20 nm, space of 2 μm, height of 250 nm). b) Reflection POM images of uniformly aligned dendrimer cylinders within the patterned area by rotation at −45° and +45° to the polarizer. Reflection POM images under a 530 nm 1λ wave plate by rotation at −45° and +45° to the polarizer. c) The GISAXS pattern of dendrimer cylinders confined in line patterns. The incident X-ray beam was either parallel to the pattern direction (left) or perpendicular to the pattern direction (right). d) AFM image of the line patterned area filled with dendrimer cylinders and the corresponding FFT images of each marked position.

the FFT patterns in the lateral positions (perpendicular to the line axis, green spots) revealed that the orientation direction of the dendrimer cylinders is identical to the guiding template. Notably, this ordering behavior was not limited to the marked region, and the dendrimer cylinders were aligned parallel along the line patterns at arbitrary positions over the entire patterned area.

To understand the effects of the ratio of pattern height to film thickness on the orientation of the cylinders, the precise thickness control of the dendrimer film in the pattern template was achieved by varying the dendrimer solution concentration and maintaining consistent guiding template dimensions. **Figure 3** shows the alignment of the dendrimer cylinders confined in the patterned line template ($w \approx 20$ nm, $s \approx 2$ μm, $h \approx 250$ nm) with variation in the ratio of the dendrimer film thickness (t) to the pattern height (h). When a dendrimer cylinder was filled in a high-resolution line pattern with $t/h \approx 0.5$ (at a dendrimer thickness of ≈120 nm and a dendrimer solution concentration of 1 wt%), uniform blue POM images were observed for the dendrimer film filled in the line pattern, which was rotated at −45° to the polarizer in the presence of the 1λ wave plate (Figure 3a, top). These results revealed the uniform alignment of the dendrimer cylinders over large areas. AFM height images confirmed that the dendrimer cylinders are parallel to the line patterns over large areas (Figure 3a, middle). Bottom of Figure 3a shows a schematic of the cylinder alignments along the Au line pattern direction. When a dendrimer film of a higher thickness (1.5 wt%) was filled into the line patterns within a range of $0.5 < t/h < 1$, non-uniform alignment, which corresponded to the coexistence of red and blue, was observed in the reflected POM images; this alignment possibly corresponded to the presence of a number of small domains with different orientations in the observed region (Figure 3b, top).

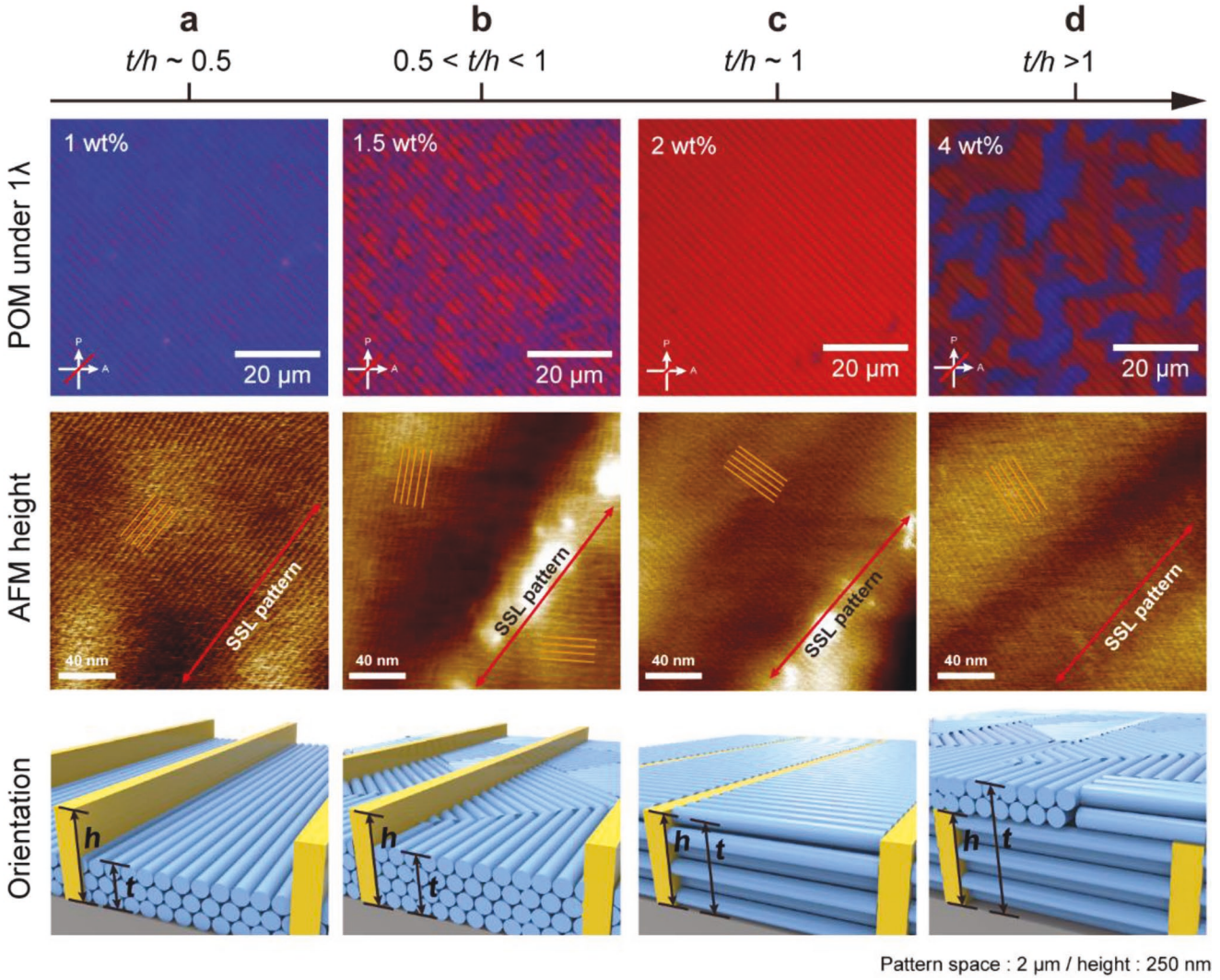

Figure 3. Alignment direction depending on the dendrimer film thickness. Characterization of aligned dendrimer cylinders with reflection POM images under a 1λ wave plate by rotation at −45° to the polarizer (top), and AFM images (middle) corresponding to the reflection POM images. Schematics of aligned dendrimer cylinders depending on the ratio of the dendrimer film thickness (t) to the pattern height (h) (bottom). a) The dendrimer cylinders confined in line patterns (w ≈20 nm, s ≈2 μm, h ≈250 nm) with the ratio t/h ≈0.5. b) 0.5 < t/h < 1 c) t/h ≈1, and d) t/h > 1.

AFM analysis clearly revealed the presence of a cylinder array with two orientations around the line pattern (Figure 3b, middle). Although two different orientations were observed in the AFM image, a large number of different orientations existed within a single channel over a macroscopic area, as displayed in Figure 3b, bottom. Interestingly, the uniform planar orientation of the dendrimer cylinders with a long-range order was again generated when the dendrimer film was cast with the same thickness as the pattern height ($t/h \approx 1$, with a dendrimer film of 250 nm and a dendrimer solution concentration of 2 wt%). The magenta color of the POM image for the line pattern with a $t/h \approx 1$ revealed the uniform orientation of the dendrimer cylinders over large areas (Figure 3c, top). The AFM image (Figure 3c, middle) provided clear evidence for the formation of dendrimer cylinders that were oriented perpendicular to the Au line pattern (Figure 3c, bottom). When the thickness of the dendrimer film was greater than the pattern height ($t/h > 1$), relatively large domains (≈20 μm) of dendrimer cylinders with different orientations were observed in the reflection POM (Figure 3d, top) and AFM (Figure 3d, middle) images. For $t/h > 1$, dendrimer cylinders, which were located on the dendrimer film surface, might not be effectively guided by the line patterns; thus, a non-uniform planar orientation is observed as shown at the bottom of Figure 3d.

2.2. Competing Mechanisms for Alignment

The richness of the experimental scenarios investigating the alignment of the supramolecular dendrimers suggested the possibility of at least two competing mechanisms for their alignment. These mechanisms are associated with: i) the physical surface anchoring of the cylinders on the Au walls and ii) the so-called geometrical anchoring imposed by the tilted

dendrimer–air interface in the wedge-like meniscus region near Au walls; this geometrical anchoring originates from the elastic energy of the liquid crystal.

2.2.1. Physical Surface Anchoring on the Au Walls

Previously, several surfaces were reported to favor the perpendicular alignment of dendrimer cylinders.[22] This alignment was also observed in rectangular microchannels, and several surfaces (including Teflon AF, carbon, and Polyethylenimine (PEI)) favored perpendicular alignment (Figures S10 and S11, Supporting Information). Thus, it is expected that the Au vertical walls of the pattern provoke a similar homeotropic surface alignment (Figure S12, Supporting Information). Such an alignment can be characterized by the Rapini–Papoular anchoring potential in the form of $f_{anch} = \frac{1}{2} W \sin^2\phi$, where W is the surface anchoring coefficient and ϕ is the angle between the x-axis normal to the Au wall and the local director $\hat{n}$. The surface anchoring penalty for any realignment from the homeotropic alignment can be estimated per unit length of the microchannel as $F_{anch} = \frac{\alpha^2 W \bar{t}}{2} \sin^2\phi$, where $\bar{t}$ is the average thickness of the dendrimer film and $\alpha^2 \approx 1$ is a positive-definite dimensionless coefficient that accounts for a small difference between $\bar{t}$ and the actual height of the dendrimer film measured at the Au wall (which is slightly greater than $\bar{t}$ because of the meniscus geometry, **Figure 4**a–d).

2.2.2. Geometrical Anchoring Caused by the Tilted Dendrimer-Air Interface

Experiments demonstrated that when the dendrimer film is less than the height (h) of the Au walls, the dendrimer–air interface was not flat (Figure S13, Supporting Information). It was instead tilted by some nonzero angle γ with respect to the horizontal bottom substrate (Figure S14, Supporting Information). This meniscus effect was clearly observed in Figure 4a 4,b, and the dendrimer–air interface struck the Au wall at $\pi/2 - \gamma \approx 1.33$ (76°).

To preserve the tangential orientation to the air interface and bottom substrate, and to maintain the alignment close to the homeotropic alignment at the Au wall, the director must form a splay configuration, as shown in Figure 4c. If the director remains in the x-z plane, the elastic energy splay[28] is expressed as $F_{el} = \frac{K_{11} s}{2\bar{t}} \gamma^2$ per unit length of the microchannel; here, K_{11} represents the splay elastic constant (expected to be extremely high for cylinder phases[29]); and s represents the channel width. This elastic energy can dramatically decrease if the director is reoriented away from the x-z plane and aligned parallel to the Au walls. If the angle between the x-z plane and the director is denoted as is ϕ, then the elastic energy per unit area of the horizontal x-y plane is expressed as follows[28,30]:

$$F_{el} = \frac{K_{11} s}{2\bar{t}} \left[\arcsin\left(\sin\gamma \cos\phi\right)\right]^2 \quad (1)$$

For any non-zero tilt γ, the elastic energy clearly exhibited a single minimum, corresponding to $\phi = \pi/2$, that is, to the director being aligned parallel to the y-axis, and hence parallel to the Au walls (Figure 4d). This preferred orientation of the director, originating from the elastic response of the material with a tilted confinement, has been referred to as "geometrical anchoring."[28,30]

Different alignment regimes observed experimentally for different values of the ratio t/h can be explained by the balance of the two types of anchoring, as follows. The total energy per unit length of the microchannel is represented by the sum $F = F_{el} + F_{anch}$, which can be expressed for small tilts $\gamma \ll 1$ as:

$$F = \frac{\gamma^2 K_{11} s}{2\bar{t}} \cos^2\phi + \frac{\alpha^2 W \bar{t}}{2} \sin^2\phi \quad (2)$$

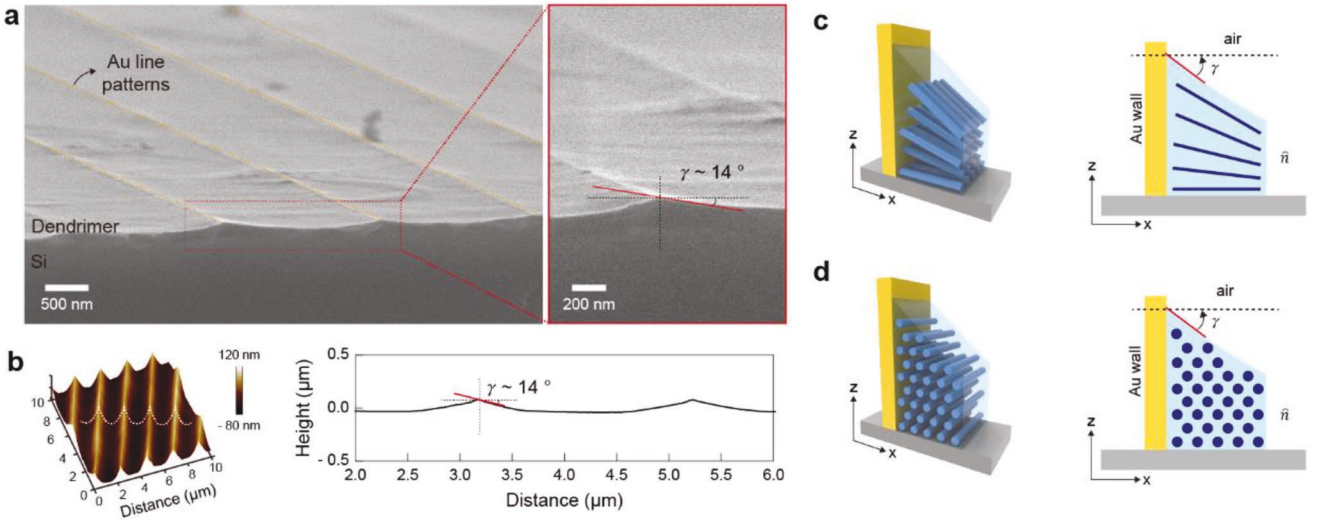

Figure 4. The meniscus of the dendrimer-air interface and the alignment direction according to elastic energy. Non-flat geometry of the dendrimer–air interface caused by a meniscus near Au walls. a) Tilted SEM image of the dendrimer–air interface. b) Calculated meniscus between the Au walls and the dendrimer film by AFM analysis. Mechanistic scheme of the geometrical anchoring at the tilted dendrimer–air interface. c) Homeotropic alignment at the Au wall resulting in splay deformations with a high elastic energy. d) Elastic energy is reduced to zero when the cylinders are aligned parallel to the Au walls; the energy cost is related to the physical surface anchoring.

The total energy minimum was clearly $\phi = \pi/2$ for a small thickness of the dendrimer film, $\overline{t} < \overline{t}_{crit}$, where the latter term is the characteristic length determined by the tilt of the interface γ and is defined as:

$$\overline{t}_{crit} = \frac{\gamma}{\alpha}\sqrt{\frac{sK_{11}}{W}} \quad (3)$$

Here, K_{11}/W is the anchoring extrapolation length. Using typical experimental values of $\gamma \approx 0.24$, $s \approx 2$ μm, and assuming $\alpha = 1$ and $K_{11}/W \approx 0.1$ μm,[27] the critical thickness of the film below which the dendrimer cylinders align perpendicularly to the Au walls, that is, at $\phi = \pi/2$, is ≈100 nm; this result is in good agreement with the experimental data. This regime corresponds to the experimental case of the cylinders aligned parallel to the patterned line axis when $t/h \approx 0.5$

If $\overline{t} > \overline{t}_{crit}$, the model above predicts that the physical surface anchoring becomes comparable to the elastic cost of deformations. Thus, the cylinders might be either parallel or perpendicular to the Au walls. This regime most likely corresponds to the experimentally observed misaligned textures for $0.5 < t/h < 1$. When $t/h \approx 1$, the meniscus tilt angle vanishes, $\gamma \approx 0$; thus, $F_{el} = 0$, and the only energy to minimize is the physical anchoring energy, $F_{anch} = \frac{\alpha^2 w\overline{t}}{2}\sin^2\phi$, which yields $\phi = 0$, that is, cylinders aligned perpendicularly to the Au walls, as observed in the experiments (Figure S15, Supporting Information). Finally, when $t/h > 1$, the alignment action of the Au walls diminished as the area of contact between Au and the dendrimers decreased, and the alignment became irregular (Figure 3).

Our study represents the ordering behavior of the dendrimer cylinders in line patterns comprising Au on a Si substrate, the patterns of which were not subjected to surface modification. This investigation did not completely explain the ordering behavior of dendrimer cylinders depending on various surface properties of line patterns and bottom substrates, but it demonstrated the directing mechanism to better understand the DSA of dendrimer cylinders.

2.3. Alignment of Dendrimer Cylinders with Bent Line Patterns

To investigate the feasibility of the DSA of dendrimer cylinders with a directed line axis, a 150° bent line pattern with a high aspect ratio (w ≈20 nm, s ≈2 μm, h ≈300 nm) was designed (**Figure 5**a). A dendrimer solution (1 wt%) in chloroform was created and spin-coated onto the patterned area, and the dendrimer film was then cooled from its isotropic melt state to room temperature at a rate of 1 °C min^{-1} to obtain a continuous alignment direction along the line patterns. After cooling, the alignment of the 100-nm-thick dendrimer cylinders filled in the patterned area, as was confirmed by the AFM images (Figure 5b). The meniscus between the dendrimer film and air interface near the Au wall was clearly observed, where the tilted angle of the dendrimer–air interface was 19°. The tilted angles of the dendrimer–air interface near the Au walls were the same at any position at which the meniscus was measured, including near the angled patterns (Figure S16, Supporting Information). Figure 5c shows a series of AFM images of the dendrimer cylinders in five regions of the 150° bent line patterns. AFM was used for the direct observation of the oriented dendrimer cylinder, which was confined in the line pattern. Notably, the dendrimer cylinders, which were located inside the curved line pattern, bent smoothly along the line axis without significant defects. The connected line of five white arrows (Figure 3c), which indicates the representative orientation of a cylinder in each region, exhibited the same curvature of the 150° bent line patterns. Moreover, the highly magnified AFM image of position 3 clearly revealed bent dendrimer cylinders along the curved guide pattern. To demonstrate that the orientation of the cylinder was effectively guided by the high-resolution pattern in the non-planar dimension, average directional angles of the cylinder, which were obtained from five regions on the curved area, were analyzed. The average direction of the dendrimer cylinder, existing inside the pattern of the observed region, is represented as a normal line (red line, A) with respect to the connection line (blue line) between two spots of the corresponding FFT patterns. The average directional angle (Φ) is defined as the angle between the red normal line (A) and the vertical line (B). The average direction angle (Φ) from position 1 to position 5 changed from 12.49° to −17.47°. Particularly, the directional angle difference of positions 1 and 5 was 29.97°; this value matches the angle difference (≈30°) of the guide patterns of positions 1 and 2, thereby providing additional evidence that the direction of the ordered dendrimer cylinders follows the guide pattern.

3. Conclusion

In this study, a method for the DSA of supramolecular dendrimers with a high resolution (<5 nm) by graphoepitaxy was successfully developed. Cylinders from supramolecular dendrimer films with a high resolution exhibited a planar ordering with long-range lateral (>4 cm × 4 cm) order via topographical templates with a high aspect ratio (>10) and high spatial resolution (≈20 nm). The alignment direction of the cylinders was critically dependent on the ratio of the dendrimer film thickness (t) to the pattern height (h) of the guiding template. The dendrimer cylinder exhibited a parallel planar orientation along the guiding line at $t/h \approx 0.5$, whereas it exhibited a perpendicular orientation with respect to the line template at $t/h \approx 1$. Theoretical calculations demonstrated that this result is related to two competing mechanisms: i) the physical surface anchoring of the cylinders on the Au walls and ii) the geometrical anchoring imposed by the tilted dendrimer–air interface, originating from the elastic energy of the liquid crystal. Hence, the orientation of a high-resolution dendrimer cylinder over a macroscopic area was achieved by guiding topographical templates, with a high aspect ratio and spatial resolution, via simple thickness control.

The remained challenges of supramolecular structures, which have to be solved for nanolithography, are the formation of a monolayer film and pattern transfer to a substrate. After accomplishing these challenges, dendrimer-based bottom-up lithography will be a potential technique to generate dense areal packing of sub-5 nm patterns. Furthermore, supramolecular templating method is expected to be applied for different supramolecules,

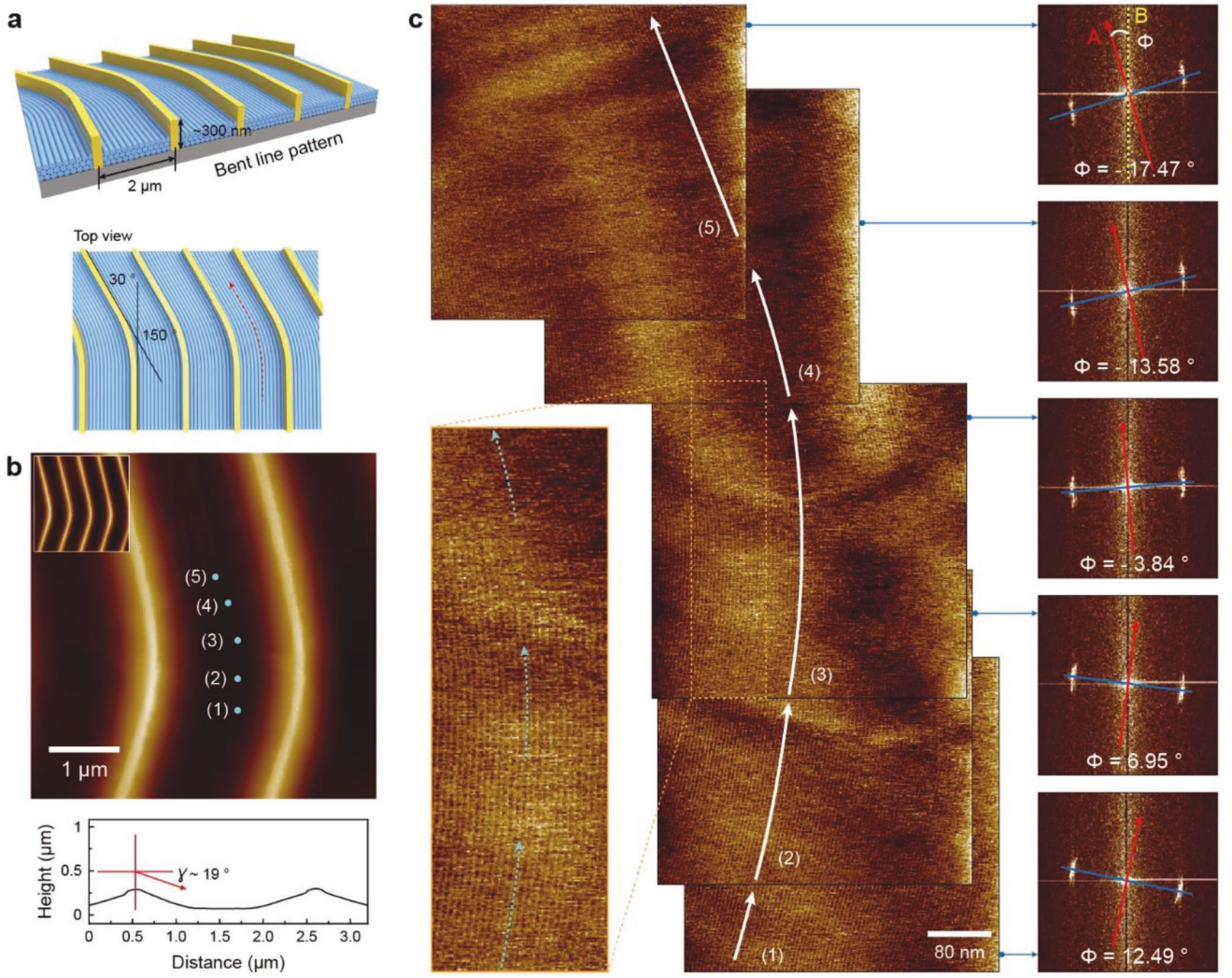

Figure 5. Alignment of dendrimer cylinders with bent line patterns. a) Schematic of the aligning dendrimer cylinders by the 150° bent line patterns of a high aspect ratio (width of 20 nm, space of 2 μm, height of 300 nm). b) AFM images of the dendrimer films filled in the 150° bent line patterns and measured meniscus at the dendrimer–air interface near the Au walls by AFM analysis. c) Continuous AFM images and the corresponding FFT images of the dendrimer cylinders along the bent line patterns.

such as cubic, hexagonal, lamellae, and other complex structures, then various sub-5 nm pattern designs will be proposed.

4. Experimental Section

Materials: A taper-shape dendrimer, propyl 3,4,5-tris(3,4,5-tris(4-(dodecyloxy)benzyloxy) benzyloxy)benzoate, was synthesized according to a previously reported method (Figures S1 and S2, Supporting Information).[22,31] The phase transition was described as follows: Cr. −22 °C, Col_h 86 °C, Iso.

Preparation of a Silicon Trench: Rectangular microchannels were fabricated on Si(100) wafers by photolithography, the features of which were controlled by tuning the wet etching conditions.[32]

Preparation of High-Aspect-Ratio Line Patterns: A polystyrene (PS) film (M_w = 18000 g mol^{-1}, 5 wt% solution in anhydrous toluene) was spin-coated on a silicon wafer comprising a native oxide layer (≈20 nm). A polydimethylsiloxane (PDMS) mold (Sylgard 184 and curing agent, 10:1 by weight, Dow Corning), which was replicated from the silicon pattern (width of 1 μm, space of 1 μm, depth of 600 nm), was placed on the PS film. The PS film was filled into the spaces of the PDMS mold above the glass transition temperature (135 °C) under vacuum conditions. The 20-nm gold film was deposited onto the PS pre-pattern by e-beam evaporation. The gold film was deposited on the sidewall of the PS pre-pattern by Ar^+ ion milling. The PS pre-pattern was removed by reactive ion etching (RIE, O_2, 100 sccm, 20 mTorr). High-aspect-ratio line patterns were obtained after the removal of the PS pre-pattern.

Alignment of Dendrimer Cylinders: The dendrimer solution (dissolved in chloroform (Aldrich)) was spin-coated (3000 rpm, 30 s) onto the line patterns. Samples heated above the isotropic temperature (87 °C) using a hot stage (LTS350, Linkam) were cooled to the room temperature at a rate of 1 °C min^{-1}.

Characterization: Textures of the dendrimer-based cylindrical structures were observed by polarized optical microscopy (LV-100POL, Nikon) equipped with a 530 nm 1λ wave plate and a charge-coupled device (CCD) camera. Surface morphologies of the cylindrical structures and the dendrimer film thickness were observed by tapping-mode atomic force microscopy (AFM, Bruker, Multimode-8). AFM images were analyzed by Nanoscope analysis. Scanning electron microscopy (SEM, S-5000, Hitachi) images were recorded to observe the dendrimer–

air interface near the Au walls. GISAXS measurement was carried out at the Pohang Accelerator Laboratory (PAL) with the small-angle X-ray scattering (3C1 SAXS) beamline.

Supporting Information

Supporting Information is available from the Wiley Online Library or from the author.

Acknowledgements

K.P., W.-B.J., K.K. contributed equally to this work. O.D.L. conducted theoretical studies. This study was supported by the Pohang Accelerator Laboratory (PAL) using the small-angle X-ray scattering (3C1 SAXS) beamline. This study was supported by the Samsung Research Funding Center of Samsung Electronics under Project number SRFC-MA1502-04. This study was supported by the National Research Foundation of Korea (NRF) grant funded by the Ministry of Science, ICT and future Planning, Korea (MSIP, NRF-2018R1A2B3008658) and the KAIST GCORE(Global Center for Open Research with Enterprise) grant funded by the Ministry of Science and ICT (N11180214). This study was supported by NSF grants DMR-1507637 and DMREF DMS-1729509.

Conflict of Interest

The authors declare no conflict of interest.

Keywords

dendrimer building blocks, directed self-assembly, geometrical anchoring, planar alignment, topographical patterns

Received: March 3, 2019
Revised: April 1, 2019
Published online:

[1] a) J. Bang, U. Jeong, D. Y. Ryu, T. P. Russell, C. J. Hawker, *Adv. Mater.* **2009**, *21*, 4769; b) C. Cummins, T. Ghoshal, J. D. Holmes, M. A. Morris, *Adv. Mater.* **2016**, *28*, 5586.

[2] a) S.-M. Yang, S. G. Jang, D.-G. Choi, S. Kim, H. K. Yu, *Small* **2006**, *2*, 458; b) J. Zhang, Y. Li, X. Zhang, B. Yang, *Adv. Mater.* **2010**, *22*, 4249.

[3] Y. H. Kim, D. K. Yoon, H. S. Jueong, O. D. Lavrentovich, H.-T. Jung, *Adv. Funct. Mater.* **2011**, *21*, 610;

[4] a) K. Nickmans, A. P. H. J. Schenning, *Adv. Mater.* **2018**, *30*, 1703713; b) Y. H. Kim, D. K. Yoon, H.-T. Jung, *J. Mater. Chem.* **2009**, *19*, 9091.

[5] a) F. S. Bates, G. H. Fredrickson, *Annu. Rev. Phys. Chem.* **1990**, *41*, 525; b) L. Leibler, *Macromolecules* **1980**, *13*, 1602.

[6] S. J. Jeong, J. Y. Kim, B. H. Kim, H. S. Moon, S. O. Kim, *Mater. Today* **2013**, *16*, 468.

[7] a) S. O. Kim, H. H. Solak, M. P. Stoykovich, N. J. Ferrier, J. J. de Pablo, P. F. Nealey, *Nature* **2003**, *424*, 411; b) E. W. Edwards, M. F. Montague, H. H. Solak, C. J. Hawker, P. F. Nealey, *Adv. Mater.* **2004**, *16*, 1315.

[8] a) B. H. Kim, J. Y. Kim, S. J. Jeong, J. O. Hwang, D. H. Lee, D. O. Shin, S. Y. Choi, S. O. Kim, *ACS Nano* **2010**, *4*, 5464; b) P. Mansky, Y. Liu, E. Huang, T. P. Russell, C. J. Hawker, *Science* **1997**, *275*, 1458.

[9] a) H. S. Suh, D. H. Kim, P. Moni, S. S. Xiong, L. E. Ocola, N. J. Zaluzec, K. K. Gleason, P. F. Nealey, *Nat. Nanotechnol.* **2017**, *12*, 575; b) E. Yoon, E. Kim, D. Kim, J. G. Son, *Adv. Funct. Mater.* **2015**, *25*, 913.

[10] a) R. A. Segalman, H. Yokoyama, E. J. Kramer, *Adv. Mater.* **2001**, *13*, 1152; b) D. Sundrani, S. B. Darling, S. J. Sibener, *Nano Lett.* **2004**, *4*, 273; c) Y. S. Jung, C. A. Ross, *Nano Lett.* **2007**, *7*, 2046.

[11] a) H. Q. Xiang, K. Shin, T. Kim, S. I. Moon, T. J. McCarthy, T. P. Russell, *Macromolecules* **2004**, *37*, 5660; b) P. Dobriyal, H. Q. Xiang, M. Kazuyuki, J. T. Chen, H. Jinnai, T. P. Russell, *Macromolecules* **2009**, *42*, 9082.

[12] a) D. E. Angelescu, J. H. Waller, D. H. Adamson, P. Deshpande, S. Y. Chou, R. A. Register, P. M. Chaikin, *Adv. Mater.* **2004**, *16*, 1736; b) D. E. Angelescu, J. H. Waller, R. A. Register, P. M. Chaikin, *Adv. Mater.* **2005**, *17*, 1878.

[13] a) M. L. Wu, D. Wang, L. J. Wan, *Nat. Commun.* **2016**, *7*, 10752; b) T. Xu, A. V. Zvelindovsky, G. J. A. Sevink, K. S. Lyakhova, H. Jinnai, T. P. Russell, *Macromolecules* **2005**, *38*, 10788.

[14] a) Y. Rokhlenko, M. Gopinadhan, C. O. Osuji, K. Zhang, C. S. O'Hern, S. R. Larson, P. Gopalan, P. W. Majewski, K. G. Yager, *Phys. Rev. Lett.* **2015**, *115*, 258302; b) M. Gopinadhan, Y. Choo, K. Kawabata, G. Kaufman, X. D. Feng, X. J. Di, Y. Rokhlenko, L. H. Mahajan, D. Ndaya, R. M. Kasi, C. O. Osuji, *Proc. Natl. Acad. Sci. USA* **2017**, *114*, E9437.

[15] M. Muramatsu, T. Nishi, G. You, Y. Saito, Y. Ido, N. Oikawa, T. Tobana, K. Ito, S. Morikita, T. Kitano, *Proc. SPIE* **2017**, *10144*, 101440Q.

[16] a) J. W. Jeong, Y. H. Hur, H. J. Kim, J. M. Kim, W. L. Park, M. J. Kim, B. J. Kim, Y. S. Jung, *ACS Nano* **2013**, *7*, 6747; b) Y. H. Hur, S. W. Song, J. M. Kim, W. I. Park, K. H. Kim, Y. Kim, Y. S. Jung, *Adv. Funct. Mater.* **2018**, *28*, 1800765.

[17] a) B. M. Rosen, C. J. Wilson, D. A. Wilson, M. Peterca, M. R. Imam, V. Percec, *Chem. Rev.* **2009**, *109*, 6275; b) H. J. Sun, S. D. Zhang, V. Percec, *Chem. Soc. Rev.* **2015**, *44*, 3900.

[18] K. Kwon, B. L. Suh, K. Park, J. Kim, H.-T. Jung, *Sci. Rep.* **2019**, *9*, 3385.

[19] a) X. Feng, K. Kawabata, G. Kaufman, M. Elimelech, C. O. Osuji, *ACS Nano* **2017**, *11*, 3911; b) J. A. M. Lugger, D. J. Mulder, S. Bhattacharjee, R. P. Sijbesma, *ACS Nano* **2018**, *12*, 6714.

[20] a) H.-T. Jung, S. O. Kim, Y. K. Ko, D. K. Yoon, *Macromolecules* **2002**, *35*, 3717; b) D. A. Barkley, T. Koga, J. G. Rudick, *Macromolecules* **2015**, *48*, 2849.

[21] a) P.-O. Mouthuy, S. Melinte, Y. H. Geerts, A. M. Jonas, *Nano Lett.* **2007**, *7*, 2627; b) R.-B. Zhang, X.-B. Zeng, C. Wu, Q. Jin, Y. Liu, G. Ungar, *Adv. Funct. Mater.* **2019**, *29*, 1806078.

[22] K. Kwon, J. M. Ok, Y. H. Kim, J. S. Kim, W. B. Jung, S. Y. Cho, H. T. Jung, *Nano Lett.* **2015**, *15*, 7552.

[23] a) D. Miyajima, F. Araoka, H. Takezoe, J. Kim, K. Kato, M. Takata, T. Aida, *Angew. Chem., Int. Ed.* **2011**, *50*, 7865; b) D. K. Yoon, S. R. Lee, Y. H. Kim, S.-M. Choi, H.-T. Jung, *Adv. Mater.* **2006**, *18*, 509; c) X. Feng, M. E. Tousley, M. G. Cowan, B. R. Wiesenauer, S. Nejati, Y. Choo, R. D. Noble, M. Elimelech, D. L. Gin, C. O. Osuji, *ACS Nano* **2014**, *8*, 11977.

[24] a) K. Nickmans, J. N. Murphy, B. de Waal, P. Leclere, J. Doise, R. Gronheid, D. J. Broer, A. P. H. J. Schenning, *Adv. Mater.* **2016**, *28*, 10068; b) K. Nickmans, G. M. Bögels, C. Sánchez-Somolinos, J. N. Murphy, P. Leclère, I. K. Voets, A. P. H. J. Schenning, *Small* **2017**, *13*, 1701043.

[25] H. J. Jeon, K. H. Kim, Y. K. Baek, D. W. Kim, H. T. Jung, *Nano Lett.* **2010**, *10*, 3604.

[26] a) W. B. Jung, H. S. Jeong, H. J. Jeon, Y. H. Kim, J. Y. Hwang, J. H. Kim, H. T. Jung, *Adv. Mater.* **2015**, *27*, 6760; b) H. S. Jeong, H. J. Jeon, Y. H. Kim, M. B. Oh, P. Kumar, S. W. Kang, H. T. Jung, *NPG Asia Mater.* **2012**, *4*, e7.

[27] a) J. Cattle, P. Bao, J. P. Bramble, R. J. Bushby, S. D. Evans, J. E. Lydon, D. J. Tate, *Adv. Funct. Mater.* **2013**, *23*, 5997; b) J. P. Bramble, D. J. Tate, D. J. Revill, K. H. Sheikh, J. R. Henderson, F. Liu, X. B. Zeng, G. Ungar, R. J. Bushby, S. D. Evans, *Adv. Funct. Mater.* **2010**, *20*, 914.
[28] O. D. Lavrentovich, *Phys. Rev. A* **1992**, *46*, R722.
[29] M. Kleman, O. D. Lavrentovich, *Soft Matter Physics: An Introduction*, Springer, New York **2004**.
[30] L. Tortora, O. D. Lavrentovich, *Proc. Natl. Acad. Sci. USA* **2011**, *108*, 5163.
[31] a) V. Percec, W.-D. Cho, P. E. Mosier, G. Ungar, D. J. P. Yeardley, *J. Am. Chem. Soc.* **1998**, *120*, 11061; b) V. Percec, M. Glodde, T. K. Bera, Y. Miura, I. Shiyanovskaya, K. D. Singer, V. S. K. Balagurusamy, P. A. Heiney, I. Schnell, A. Rapp, H. W. Spiess, S. D. Hudson, H. Duan, *Nature* **2002**, *419*, 384; c) E. Pouzet, V. De Cupere, C. Heintz, J. W. Andreasen, D. W. Breiby, M. M. Nielsen, P. Viville, R. Lazzaroni, G. Gbabode, Y. H. Geerts, *J. Phys. Chem. C* **2009**, *113*, 14398.
[32] J. Fruhauf, S. Kronert, *Microsyst. Technol.* **2005**, *11*, 1287.